TECHNISCHE MECHANIK, 32, 6, (2012), 631 - 648
submitted: February 02, 2011

A Study of Ductile Damage and Failure of Pure Copper – Part II: Analysis of the Deep Drawing Process of a Cylindrical Shell

M. Zapara, N. Tutyshkin, W.H. Müller, R. Wille

The analysis of the stress-strain state and strain induced damage of a cylindrical shell made of copper during the process of deep drawing is presented. The stresses on the contact surface of operating tools (punch and die) are assigned implicitly, which leads to the mixed boundary-value problem. The results are obtained on the basis of the solution of the constitutive differential equations presenting plane plastic flow in curvilinear characteristic coordinates. The material functions required for the analysis of deep drawing were obtained by experimental studies of ductile damage and failure of pure copper (cf., Zapara et al., 2011). The process of deformation with discontinuities of the tangential velocities at the plastic zone boundaries is discussed. An estimate of the local strains and damage in the material is given both for the plastic zone and for its boundaries. The distributions of strains and of the damage within the wall of a finished part are determined. These distributions strongly affect the strength properties of a shell. The modeling of ductile damage in a material during deep drawing is based on experimental results and considerably extends them for a wider range of stress triaxialities. It is shown that the use of a drawing die with a cone angle of $12^\circ...13^\circ$ leads to a noticeable shift of the stress triaxialities into a range of negative values as compared to deep drawing with a die of larger angle ($15^\circ...18^\circ$). The modeling reveals a smoother increase and decrease in damage of the finished part in case of the smaller cone angle as well as the absence of void coalescence. This fact is very important when manufacturing such products at high operating speeds. The obtained results in combination with similar ones from the literature can be applied to the analysis of metal forming processes with dominant tensile deformation (e.g., drawing, deep drawing, strip-drawing, ironing).

1 Introduction

Drawing operations are widely used in Metal Forming (MF). Applied plasticity theory is used for the development of MF processes and allows us to determine the stress-strain fields and related process-dependent parameters as well as to predict structural and mechanical properties of finished parts. The reliable prediction of strain-induced damage including the limit state of a workpiece is very important problem in metal forming. Damage in the zones with intensive deformation depends essentially on the strain history, the stress state, and the effect of local heat release related to the energy of plastic dissipation. In this paper we study deep drawing of a copper cylindrical shell (Fig. 1). The process force, P , is transmitted from the punch to the bottom part of a shell and gives rise to the tensile stresses in its walls. Thus tensile plastic strains dominate in the material during deep drawing. This fact allows us to predict strain induced damage in deep-drawn parts by using the experimental results obtained from uniaxial tension tests. Bonora *et al.* (2005) show a possibility in order to assess ductile damage and failure in metals in processes with non-proportional loading and changing stress triaxialities by using material parameters determined experimentally from simple tests.

Numerical methods are successfully used to solve MF problems in many cases. These methods offer many constantly increasing possibilities in the modeling of plastic deformation. One of the first numerical analyses of sheet MF processes was done by Woo (1965), who considered the material as isotropic and used a finite difference method to solve the case of axisymmetric punch stretching and drawing. An elastic-plastic finite element (FE) formulation of stretch forming for a punch and a die of arbitrary shape was introduced by Wang and Budiansky (1978). Oh *et al*. (1979) applied the modified Cockcroft and Latham tensile plastic work criterion and modified McClintock's void growth criterion in order to predict the occurrence of central bursting in axisymmetric drawing and extrusion by using the rigid-plastic FE formulation. The critical values of material parameters appearing in the fracture criteria were obtained from tension/compression experiments. Many researchers (*cf.*, *e.g*., Gelin, *et al*., 1985; Aravas, 1986; Bennani and Oudin, 1995) used Gurson's plastic potential (*cf*., Gurson, 1977) for a description of ductile damage in various metal forming processes. All of them made use of a critical void volume fraction as a fracture initiation criterion. Mathur and Dawson (1987) used a constitutive equation with an internal state variable for modeling the plastic flow and damage development in metals during

drawing operation. They used a void growth damage model proposed by Cocks and Ashby (1980) to predict the evolution of internal porosity. Damage accumulation due to the creation of new voids is neglected. Kobayashi *et al*. (1989) has worked on several sheet forming problems including drawing, bulging, stretch forming and bending using an incremental strain theory; in their work the material was assumed as rigid-plastic and work-hardening characteristics were included. Alberti *et al*. (1993) carried out an analysis of drawing process by employing the plastic potentials proposed by Gurson (1977), Needleman and Tvergaard (1984), and Oyane *et al*. (1980) for the prediction of the onset of the central burst. The critical value of void volume fraction at fracture initiation was obtained from a tension test. Their numerical predictions are in good agreement with the experimental results. Alberti *et al*. (1994) used Oyane's criterion to predict central bursting in drawing with the help of a rigid-plastic FE formulation. The material-dependent constants in the criterion were determined from compression tests. They also performed experiments by using an ultrasonic control system for detecting the defects. Tang *et al*. (1994) used the FE-code DEFORM to predict chevron defects in the drawing operation along with Cockcroft and Latham's criterion. Hsu and Chu (1995) employed a total Lagrangian formulation and a virtual work theory for the analysis of axisymmetric sheet metal forming processes. We should note that only a few important publications are mentioned above, otherwise the list could be very long and could be a subject of the independent paper. Interested readers can be referred to Reddy *et al*. (2000) for a detailed survey of the publications on this problem.

We should note several important papers that were published within last ten years and deal specifically with the modeling of deep drawing. Reddy *et al*. (2000) develop a continuum damage mechanics model for void growth and micro-crack initiation based on the microscopic phenomena of void nucleation, growth, and coalescence and use this model to predict the fracture initiation in deep drawing (*i.e*., central bursting). They also obtain a generalized strain and damage distribution by using the critical damage criteria. Hu *et al*. (2000) incorporate void nucleation and growth models into the FE-code ABAQUS together with an anisotropic fourth-order strain rate potential so that the damage evolution during deep drawing of textured aluminum sheets can be analyzed. They reveal the influence of plastic anisotropy together with that of void nucleation and growth on damage evolution for cold rolled as well as cold rolled and annealed aluminum sheets. A damage mechanics model proposed by Chow *et al.* (2003) for the prediction of localized necking and failure of sheet metals has been incorporated into the FE-code LS-DYNA. The modified program has been successfully applied to simulate both single-step and two-step forming processes, including deep drawing. The forming limit strains are predicted for both proportional and non-proportional loading conditions, and they are found to be in agreement with the test results. Guo *et al*. (2004) develop the Pseudo-Inverse Approach (PIA) by taking into account the loading history: Some realistic intermediate configurations are determined without contact treatment in order to consider the loading history. A more accurate damage rate model presented in their paper allows a strong coupling between plasticity and damage. The obtained numerical results show the feasibility of damage consideration in PIA and the influence of damage effects on the sheet formability during deep drawing. Khelifa and Oudjene (2008) present an efficient damage model based on the strong coupling of both anisotropic elasto-plasticity and isotropic ductile damage. The developed model is coupled with FEM by using ABAQUS. A comparison between numerical and experimental results is presented in the context of the square cup deep drawing benchmark test of Numisheet 1993. The results demonstrate the capability of the model to predict where and when the damaged zones will appear in the workpiece during the forming operation. Boudifa *et al*. (2009) introduce a micromechanical damage model based on crystal plasticity theory and continuum damage mechanics. They apply this model in ABAQUS to simulate the damage occurrence in deep drawing of FCC polycrystalline sheet and then present macroscopic equivalent plastic strain and damage maps for different values of the punch displacement.

However, other non-FE methods closely related to a physical mechanism of plastic deformation have always been applied to an in-depth study of forming processes. For example, the method of slip lines is successfully used to analyze the processes with plastic flow (Hill, 1950). It was experimentally shown that large defects (voids) generate microscopic slip bands (Yokobori, 1968). Therefore, determination of the slip line (or slip band) field is useful when predicting strain-induced damage and the limit state of a material before its macroscopic failure. In this paper we use a calculation technique for the strains accumulated during displacement of material particles along trajectories in the plastic zone. This method is based on mapping of flow lines onto a plane of flow velocities. The technique allows us to determine damage distribution in the wall of a finished part. In order to calculate the stresses (and stress triaxialities) in the plastic zone nodes a mixed boundary-value problem should be solved, *i.e.*, the stresses on the contact surface of operating tools (punch and die) are assigned implicitly as the relation between shear and normal stresses. The modeling results reveal that for deep-drawn shells it is appropriate to use dies with cone angles $12^{\circ}...13^{\circ}$ in order to decrease the damage and to increase the process strain. The analysis of deep drawing of a cylindrical shell made of copper includes the following steps: (i) formulation of the constitutive equations and boundary conditions (Section 2); (ii) determination of stresses

and plastic flow velocities (Section 3); (iii) calculation of the accumulated strains, ductile damage and ductile failure (Sections 4 and 5); and (iv) Section 6 contains discussion of the results .

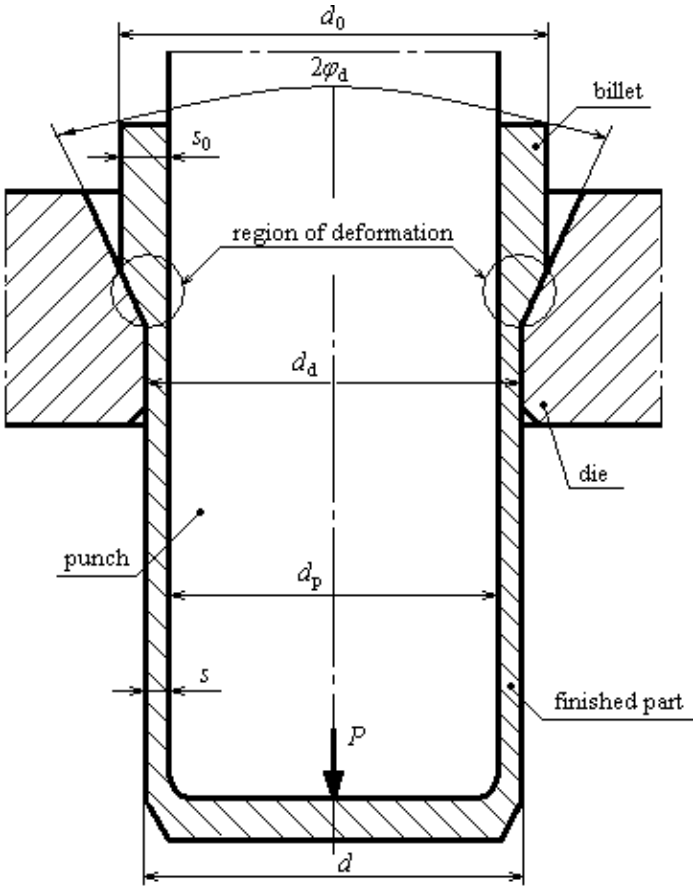

Figure 1. Deep drawing of a cylindrical shell

2 Constitutive Equations and Boundary Conditions

An axisymmetric stress-strain state occurs in the general case during deep drawing of cylindrical parts. In order to represent the axisymmetric stress-strain state completely it is sufficient to determine the fields of stresses and plastic flow velocities in the meridian cross-section of a deformed solid. The strain state is plane during the deep drawing process of a thin-walled cylindrical shell with the ratio $s/d \le 0.05$ between its thickness (s) and diameter (d) since the hoop strain is infinitely small (*cf*., Hill, 1950). This condition allows us to reduce an axisymmetric strain problem to a particular plane strain problem and to describe the stress-strain state of a shell in plane Cartesian coordinates x, y (Fig. 2) by the differential equations of equilibrium

$$\frac{\partial \sigma_x}{\partial x} + \frac{\partial \tau_{xy}}{\partial y} = 0 \ , \quad \frac{\partial \tau_{xy}}{\partial x} + \frac{\partial \sigma_y}{\partial y} = 0 \ , \tag{1}$$

the von Mises yield surface

$$(\sigma_x - \sigma_y)^2 + 4\tau_{rz}^2 = 4\tau_y^2 \ , \tag{2}$$

the condition of coaxiality of the deviatoric strain rates, $\dot{e}_{ij}$, and the deviatoric stresses, s_{ij}

$$\frac{\partial \upsilon_x / \partial x - \partial \upsilon_y / \partial y}{\partial \upsilon_x / \partial y + \partial \upsilon_y / \partial x} = \frac{\sigma_x - \sigma_y}{2\tau_{xy}} \ , \tag{3}$$

and the incompressibility condition

$$\frac{\partial \upsilon_x}{\partial x} + \frac{\partial \upsilon_y}{\partial y} = 0\,, \tag{4}$$

where σ_x, σ_y, τ_{xy} are nonzero components of the stress tensor σ_{ij}, $\tau_{\mathrm{y}} = \sigma_{\mathrm{y}}/\sqrt{3}$ is the yield stress at shear and υ_x, υ_y are the components of the vector of plastic flow velocity, υ.

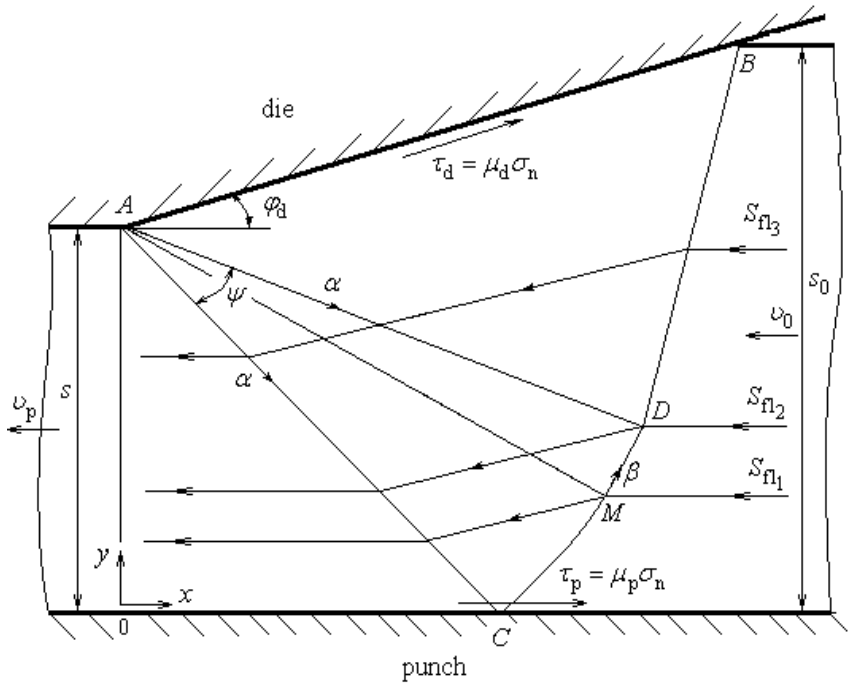

Figure 2. Plastic zone (boundary conditions, slip lines and movement trajectories of material particles) for the following initial data: $s_0/s = 1.6$, $\varphi_{\mathrm{d}} = 18^\circ$, $\mu_{\mathrm{p}} = 0.1$, $\mu_{\mathrm{d}} = 0.09$

The parametric representation of stresses for a perfectly rigid-plastic material

$$\sigma_x = \sigma_{\mathrm{H}} - \tau_{\mathrm{y}} \sin 2\delta \;\;,\;\; \sigma_{\mathrm{y}} = \sigma_{\mathrm{H}} + \tau_{\mathrm{y}} \sin 2\delta \;,\;\; \tau_{xy} = \tau_{\mathrm{y}} \cos 2\delta \tag{5}$$

leads to the following form of Eqs. (1-4)

$$\frac{\partial \sigma_{\mathrm{H}}}{\partial x} - 2\tau_{\mathrm{y}}\left(\frac{\partial \delta}{\partial x}\cos 2\delta + \frac{\partial \delta}{\partial y}\sin 2\delta\right) = 0 \;\;,\;\; \frac{\partial \sigma_{\mathrm{H}}}{\partial y} - 2\tau_{\mathrm{y}}\left(\frac{\partial \delta}{\partial x}\sin 2\delta - \frac{\partial \delta}{\partial y}\cos 2\delta\right) = 0\,, \tag{6}$$

and

$$\frac{\partial \upsilon_x}{\partial x} - \frac{\partial \upsilon_y}{\partial y} + \left(\frac{\partial \upsilon_x}{\partial y} + \frac{\partial \upsilon_y}{\partial x}\right)\tan 2\delta = 0 \;\;,\;\; \frac{\partial \upsilon_x}{\partial x} + \frac{\partial \upsilon_y}{\partial y} = 0\,. \tag{7}$$

These four Equations (6) and (7) are of the hyperbolic type and have two pair-wise coincident sets of mutually orthogonal characteristic lines

$$\frac{\mathrm{d}y}{\mathrm{d}x} = \tan\delta \;\; (\alpha \text{ - characteristics}) \,,\;\; \frac{\mathrm{d}y}{\mathrm{d}x} = -\cot\delta \;, (\beta \text{ - characteristics}), \tag{8}$$

where δ is the angle between the *x*-axis and the tangent to the characteristic line α in each material point of the plastic zone.

The characteristic lines coincide with the slip lines and form a grid of mutually orthogonal curves, α and β, in the plastic zone. Eqs. (6) and (7) can be rewritten in the curvilinear coordinates α and β as follows:

$$\mathrm{d}\sigma_{\mathrm{H}} - 2\tau_{\mathrm{y}}\,\mathrm{d}\delta = 0 \;\; (\text{along the lines } \alpha),\;\; \mathrm{d}\sigma_{\mathrm{H}} + 2\tau_{\mathrm{y}}\,\mathrm{d}\delta = 0 \;\; (\text{along the lines } \beta), \tag{9}$$

$$\mathrm{d}\upsilon_\alpha - \upsilon_\beta\,\mathrm{d}\delta = 0 \quad \text{(along the lines } \alpha\text{)}, \quad \mathrm{d}\upsilon_\beta + \upsilon_\alpha\,\mathrm{d}\delta = 0 \quad \text{(along the lines } \beta\text{)}. \tag{10}$$

Eqs. (9) can be rewritten in the integral form

$$\sigma_\mathrm{H}/2\tau_\mathrm{y} - \delta = \xi(\beta) \quad \text{(along the lines } \alpha\text{)}, \quad \sigma_\mathrm{H}/2\tau_\mathrm{y} + \delta = \eta(\alpha) \quad \text{(along the lines } \beta\text{)} \tag{11}$$

and are known as the Hencky plasticity integrals (*cf*., Hencky, 1923) while Eqs. (10) are known as the Geiringer correlations (*cf*., Geiringer, 1930). The parameters $\xi(\beta)$ and $\eta(\alpha)$ in Eq. (11) can be determined from boundary conditions. For example, if the hydrostatic stress $\sigma_{\mathrm{H}C}$ and the parametric angle δ_C are known in the boundary point C on the contact with a punch (Fig. 2) then for slip lines α (lines AC) and β (lines CDB) which pass through the point C we may write: $\xi(\beta) = \sigma_{\mathrm{H}C}/2\tau_\mathrm{y} - \delta_C$, $\eta(\alpha) = \sigma_{\mathrm{H}C}/2\tau_\mathrm{y} + \delta_C$. The averaged shear yield stress τ_y can be derived from the condition of constant plastic strain energy density for a hardened material and from the assumed model of a perfectly rigid-plastic material with the yield stress $\sigma_{\mathrm{y_m}}$ (Fig. 3). The area element $\mathrm{d}w_\mathrm{p} = \sigma_\mathrm{y}(\varepsilon_\mathrm{eq})\mathrm{d}\varepsilon_\mathrm{eq}$ under the stress-strain curve $\sigma_\mathrm{y}(\varepsilon_\mathrm{eq})$ defines an increment of plastic strain energy density for a hardened material

$$\int_0^{\varepsilon_\mathrm{eq}} \sigma_\mathrm{y}(\varepsilon_\mathrm{eq})\mathrm{d}\varepsilon_\mathrm{eq} = \sigma_{\mathrm{y_m}}\varepsilon_\mathrm{eq}, \; \sigma_{\mathrm{y_m}} = \frac{1}{\varepsilon_\mathrm{eq}}\int_0^{\varepsilon_\mathrm{eq}} \sigma_\mathrm{y}(\varepsilon_\mathrm{eq})\mathrm{d}\varepsilon_\mathrm{eq}, \; \tau_\mathrm{y} = \frac{\sigma_{\mathrm{y_m}}}{\sqrt{3}}. \tag{12}$$

Under combined (disproportional) loading the equivalent accumulated strain, ε_eq, (or Odqvist parameter) can be found by integration w.r.t. the strain path (*cf*., *e.g*., Hill, 1950)

$$\varepsilon_\mathrm{eq} = \int_{s_{OM}} \dot{\varepsilon}_\mathrm{eq}\,\mathrm{d}t = \int_{s_{OM}} \mathrm{d}\varepsilon_\mathrm{eq}\,. \tag{13}$$

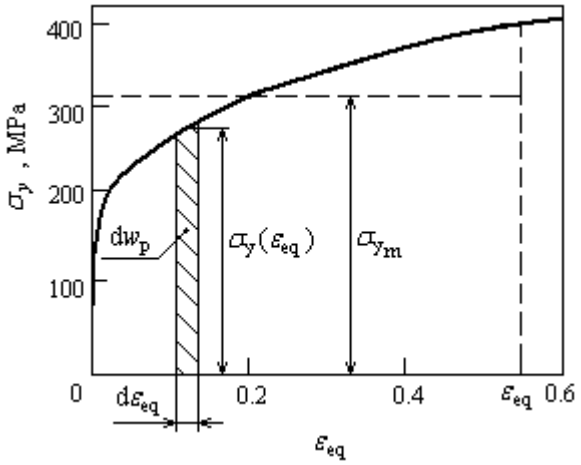

Figure 3. True stress-strain curve for pure copper

In order to calculate stresses and strains it is necessary to plot the field of slip lines (characteristics) in the plastic zone by using Eqs. (8), to find the stress parameters $\sigma_\mathrm{H}/2\tau_\mathrm{y}$ and δ in node points by Eqs. (11), and then to determine flow velocities υ_α and υ_β by Eqs. (10). The solution of the equations (8) and (11) should satisfy the boundary conditions and leads, thus, to the solution of boundary-value problems.

The boundary conditions at the contact between the processed material and the working tools are caused by friction and can be set by Coulomb's law

$$\tau_\mathrm{c} = \mu\sigma_\mathrm{n}\,, \tag{14}$$

where τ_c and σ_n denotes the shear stress and the normal pressure on the contact, respectively, the index "c" stands for contact, μ is the friction coefficient.

The boundary condition (14) leads to a complicated boundary-value problem since the stresses on the contact boundaries are specified implicitly. It is impossible to plot the slip line field directly by using Eqs. (8) since the stresses and the angle between the slip lines and the contact boundaries are unknown. A principally possible solution of similar boundary-value problems for plane plastic flow by using mappings of the boundary conditions (of the type shown in Eq. (14)) onto the stress plane σ_n, τ was initially shown by Prager and Hodge (1951). In our paper the boundary-value problem of that type is solved by mapping of the boundary conditions (12) onto the plane σ_H, τ (or onto the reduced coordinates σ_H/τ_y, τ/τ_y). The use of the mapping plane σ_H, τ (or σ_H/τ_y, τ/τ_y) instead of the plane σ_n, τ, allows us to find stress triaxialities (ST) in the mapped slip line nodes: $\mathrm{ST} = \sigma_H/\sigma_{eq} = \sigma_H/\tau_y\sqrt{3}$, where σ_H denotes the hydrostatic stress. Moreover the failure strain ε_{eq_f} that appears in the constitutive equations for ductile damage (*cf.*, Zapara *et al.*, 2011) can be determined by the failure locus ($\varepsilon_{eq_f}(\mathrm{ST})$).

In our problem the boundary conditions in terms of the stresses (14) are specified on the contact surface of the punch, $\tau_c = \mu_p\sigma_n$, and on the die, $\tau_c = \mu_d\sigma_n$. By considering Eqs. $(5)_{2,3}$ we may obtain $\tau_c = \tau_{xy} = \tau_y\cos 2\delta$ and $\sigma_n = \sigma_y = \sigma_H + \tau_y\sin 2\delta$ on the contact surface of the punch. In what follows the relation $\tau_c(\sigma_H)$ for the contact with the punch reads

$$\tau_c = \tau = \frac{\mu_p}{1+\mu_p^2}\left[\sqrt{1+\mu_p^2\left(1-\sigma_H^2\right)} - \sigma_H\right]. \tag{15}$$

For the contact surface of the die (inclined at the angle φ_d to the x-axis) we may write, respectively

$$\tau_c = \tau = \frac{\mu_d}{1+\mu_d^2}\left[\sqrt{1+\mu_d^2\left(1-\sigma_H^2\right)} - \sigma_H\right]\cos 2\varphi_d + \sqrt{1-\left[\frac{\mu_d}{1+\mu_d^2}\left[\sqrt{1+\mu_d^2\left(1-\sigma_H^2\right)} - \sigma_H\right]\right]^2}\ \sin 2\varphi_d. \tag{16}$$

In view of Eq. $(5)_3$ the Eqs. (11) allow a mapping the slip lines onto the plane σ_H, τ as follows

$$\frac{\tau}{\tau_y} = \cos 2\left[\frac{\sigma_H}{2\tau_y} - \xi(\beta)\right] \text{ (the slip lines } \alpha\text{)}, \quad \frac{\tau}{\tau_y} = \cos 2\left[-\frac{\sigma_H}{2\tau_y} + \eta(\alpha)\right] \text{ (the slip lines } \beta\text{)}. \tag{17}$$

3 Determination of Stresses and Plastic Flow Velocities

All parameters of deep drawing are calculated by using the following input data (*cf.*, Fig. 1): The material of the billet is a pure sheet copper (99.97 %); the outer diameter and the wall thickness of the initial billet and the finished part are $d_0 = 20.80$ mm, $s_0 = 1.0$ mm and $d = d_d = 19.96$ mm, $s = (d_d - d_p)/2 = (19.96 - 18.72)/2 = 0.62$ mm, respectively; the working diameters of the punch and the die are $d_p = 18.72$ mm and $d_d = 19.96$ mm, respectively; the die cone angle is $2\varphi_d = 36^\circ$; the friction coefficients on the contact surfaces of the punch and the die are $\mu_p = 0.1$ and $\mu_d = 0.09$, respectively. The billet is subjected to so-called "preforming." This operation forms a conical shape of the initial curvature between wall and bottom (*cf.*, Fig. 1). Preforming allows eliminating the peak force of deformation which might appear in the curvature during subsequent deep drawing operation, and, therefore, makes the separate analysis of deformation in the near-bottom region irrelevant.

Fig. 4 shows a mapping of the plastic flow field (the boundary conditions (15) and (16)) and the slip lines (17) onto the stress plane σ_H/τ_y, τ/τ_y for the given input data. Table 1 presents the amounts of the hydrostatic stress divided by the yield stress at shear (σ_H/τ_y), Stress Triaxiality (ST) and the parametric angle (δ) in the nodes located on the plastic zone boundary. Fig. 2 shows the corresponding slip lines including the plastic zone boundaries. According to Eqs. (11) the hydrostatic stress is constant along rectilinear segments of the slip lines. Thus, $\sigma_{HC} = \sigma_{HA}$ and $\sigma_{HD} = \sigma_{HB}$ (*cf.*, Table 1).

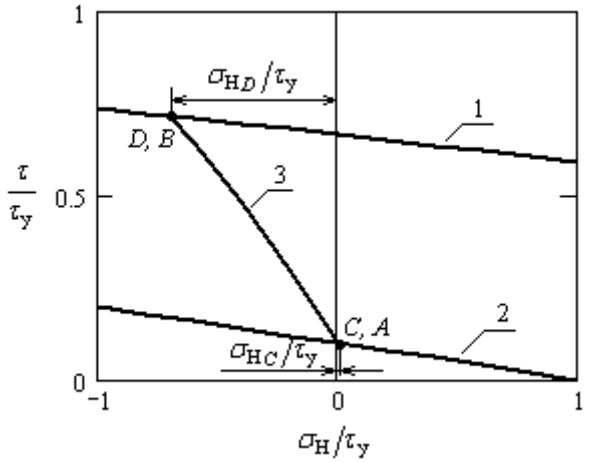

Figure 4. Mapping of the boundary conditions (15) and (16) and the slip lines (17) onto the stress plane σ_H/τ_y, τ/τ_y

Table 1. Parameters of stresses and plastic flow velocities in boundary nodes

Nodes	σ_H/τ_y	ST	δ	υ_x/υ_0	υ_y/υ_0	$\upsilon_\alpha/\upsilon_0$	$\upsilon_\beta/\upsilon_0$
A	0.012	0.009	- 0.834	-1.61	0	-1.08	-1.18
B	- 0.686	- 0.396	- 0.387	-1.00	0	-0.97	-0.35
C	0.012	0.009	- 0.834	-1.28	-0.30	-0.72	-1.18
D	- 0.686	- 0.396	- 0.387	-1.15	-.38	-0.97	-0.75

In order to determine the yield stress at shear τ_y by Eqs. (12) the true stress-strain diagram (Fig. 3) can be approximated by an exponential function $\sigma_y(\varepsilon_{eq}) = B\varepsilon^n$. For the input data given we have

$$\tau_y = \frac{1}{\varepsilon_{eq\,fin}} \int_0^{\varepsilon_{eq\,fin}} B\varepsilon_{eq}^n \mathrm{d}\varepsilon_{eq} = \frac{B}{n+1}\frac{\varepsilon_{eq\,fin}^n}{\sqrt{3}} = \frac{475}{0.271+1}\frac{0.58^{0.271}}{\sqrt{3}} = 186 \text{ MPa},$$

where the true final strain at deep drawing is $\varepsilon_{eq\,fin} = (2/\sqrt{3})\ln(F_0/F) = (2/\sqrt{3})\ln(62.2/37.7) = 0.58$.

The determined field of the slip lines α and β allows us to define the boundaries AC and BDC of the plastic zone in the meridian cross-section of the part. In order to calculate the hydrostatic stress by Eqs. (11) it is first of all necessary to find its value in one node point of the plastic zone. For this purpose, we use a condition of equilibrium of the material at the boundary CDB (that coincides with the slip line β)

$$\int_{CDB} (\sigma_H \sin\delta + \tau_{max}\cos\delta)\,\mathrm{d}s_\beta = 0, \tag{18}$$

where $\tau_{max} = \tau_y$ denotes the maximum shear stress (acting along the slip lines); $\mathrm{d}s_\beta$ is the differential of an arc of the line β. The solution of Eq. (18) allows finding the hydrostatic stress in the boundary point C (Fig. 2): $\sigma_{HC} = 2.2$ MPa ($\sigma_{HC}/\tau_y = 0.012$).

The determined field of slip lines (*i.e.*, the maximum shear stress trajectories $\tau_{a\beta}$) allows us to calculate the field of plastic flow velocities (*cf.*, Fig. 5) by using Eqs. (10). The parametric angle δ appearing in Eqs. (10) is a known function of coordinates: $\delta = \delta(\alpha, \beta)$. The field of plastic flow velocities represents the nodes of a grid of the material lines which coincide with the slip lines α and β in the coordinate system υ_r, υ_z. Such a representation allows us to find the velocity vector $\vec{\upsilon}$ and its components υ_x, υ_y (or υ_α, υ_β) for each node of the plastic zone. For example the radius vector of the represented point m is the velocity vector $\vec{\upsilon}_M$ of the material point that coincides with the point M of the slip line field, and its components are the velocity

components $\upsilon_{\alpha M}, \upsilon_{\beta M}$. The velocity field meets both the boundary conditions on the contact with the die: $\upsilon_x = -\upsilon_{\mathrm{d}} \cos\varphi_{\mathrm{d}}$, $\upsilon_y = -\upsilon_{\mathrm{d}} \sin\varphi_{\mathrm{d}}$ (with $\upsilon_{\mathrm{d}} = \upsilon_0 \cos\delta_D / \cos(\varphi_{\mathrm{d}} - \delta_D)$ denoting a scalar of the material velocity vector on the contact with the die) and the material continuity condition for the accepted scheme of plane deformation: $\upsilon_0 = (s_0/s)/\upsilon_{\mathrm{p}}$.

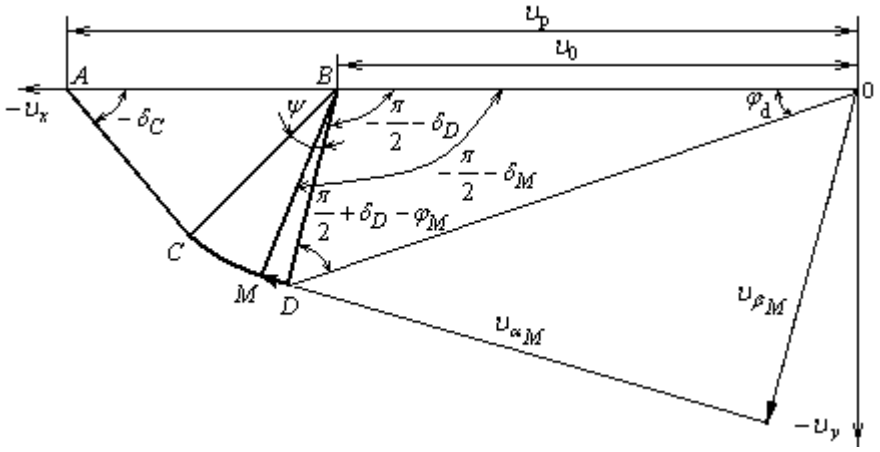

Figure 5. The field of plastic flow velocities

The boundary lines BDC and AC are lines of velocity discontinuities. When the material particles cross the boundary lines their velocities change abruptly and the tangential velocity jumps: $\Delta\upsilon_\tau = \upsilon_\tau^+ - \upsilon_\tau^-$, where υ_τ^+ and υ_τ^- are the values of the tangential velocity on both sides of the boundary. Physically speaking, the velocity discontinuity lines represent a thin ductile layer where the tangential velocity υ_τ varies strongly through the layer thickness and the normal velocity υ_{n} is constant (since its change would lead to the crack initiation). The tangential velocity discontinuity at the boundary lines BDC and AC can be defined by the length of the segments bd (or bc) and ca (Fig. 5)

$$\Delta\upsilon_{\beta\,BDC} = \upsilon_0 \frac{\sin\varphi_{\mathrm{d}}}{\cos(\varphi_{\mathrm{d}} - \delta_D)}, \quad \Delta\upsilon_{\alpha\,AC} = \upsilon_0 \frac{\sin\varphi_{\mathrm{d}}}{\cos(\varphi_{\mathrm{d}} - \delta_D)\mathrm{tg}(-\delta_C)}. \tag{19}$$

The determined field of flow velocities allows us to plot the movement trajectories of material particles according to the differential equations written in terms of α, β - coordinates: $\mathrm{d}s_\alpha = \upsilon_\alpha(\alpha, \beta, t)\mathrm{d}t$, $\mathrm{d}s_\beta = \upsilon_\beta(\alpha, \beta, t)$, where $\mathrm{d}s_\alpha$, $\mathrm{d}s_\beta$ are projections of the vector $\mathrm{d}\vec{s}_{\mathrm{tr}}$ which defines a directed increment of the trajectory $\vec{s}_{\mathrm{tr}}$ over a time period $\mathrm{d}t$. Since the deep drawing process is stationary the velocity field in the plastic zone does not change during the deformation and the velocity components that appear in the differential equations for trajectories depend only on coordinates: $\upsilon_\alpha = \upsilon_\alpha(\alpha, \beta)$, $\upsilon_\beta = \upsilon_\beta(\alpha, \beta)$. This means that the movement trajectories of material particles coincide with the corresponding flow lines s_{fl} and can be plotted by using the following equation: $\mathrm{d}s_\beta / \mathrm{d}s_\alpha = \upsilon_\beta / \upsilon_\alpha$.

An arbitrary flow line s_{fl} (which crosses the point M on the boundary BDC) can be mapped onto the plane of velocities by means of its hodograph $bmca$. The point b defines the velocity υ_0 of a particle before it enters the plastic zone, the point m defines its velocity after crossing the boundary BDC, the segment mc corresponds to a continuous change in the velocity during a particle displacement within the centered fan ABC, and the point a defines the velocity υ_{p} after crossing the boundary AC. The hodograph of flow lines allows us to calculate the strain accumulated by material particles during their movement in the plastic zone.

4 Accumulated Strains and Ductile Damage

Material particles move along their trajectories, and the strains are accumulated during this process. The hodograph of flow lines (Fig. 5) allows us to calculate the accumulated strain by using Eq. (13) as follows. The nonzero deviatoric strain increments can be written in terms of plane curvilinear coordinates α, β

$$\mathrm{d}e_\alpha = \left(\frac{\partial \upsilon_\alpha}{\partial s_\alpha} - \upsilon_\beta \frac{\partial \delta}{\partial s_\alpha}\right)\mathrm{d}t, \quad \mathrm{d}e_\beta = \left(\frac{\partial \upsilon_\beta}{\partial s_\beta} + \upsilon_\alpha \frac{\partial \delta}{\partial s_\beta}\right)\mathrm{d}t \ , \ \mathrm{d}\gamma_{\alpha\beta} = \left(\frac{\partial \upsilon_\alpha}{\partial s_\beta} - \upsilon_\beta \frac{\partial \delta}{\partial s_\beta} + \frac{\partial \upsilon_\beta}{\partial s_\alpha} + \upsilon_\alpha \frac{\partial \delta}{\partial s_\alpha}\right)\mathrm{d}t \quad (20)$$

or, according to a rule of differentiation of the vector components in curvilinear coordinates, we may have

$$\mathrm{d}e_\alpha = \frac{\mathrm{d}\upsilon_\alpha}{\mathrm{d}s_\alpha}\mathrm{d}t = \frac{\mathrm{d}\upsilon_\alpha}{\upsilon_\alpha}, \quad \mathrm{d}e_\beta = \frac{\mathrm{d}\upsilon_\beta}{\mathrm{d}s_\beta}\mathrm{d}t = \frac{\mathrm{d}\upsilon_\beta}{\upsilon_\beta} \ , \ \mathrm{d}\gamma_{\alpha\beta} = \left(\frac{\mathrm{d}\upsilon_\alpha}{\mathrm{d}s_\beta} + \frac{\mathrm{d}\upsilon_\beta}{\mathrm{d}s_\alpha}\right)\mathrm{d}t = \frac{\mathrm{d}\upsilon_\alpha}{\upsilon_\beta} + \frac{\mathrm{d}\upsilon_\beta}{\upsilon_\alpha} . \quad (21)$$

As it follows from the Geiringer relations (10), the linear strain rate in the direction of the slip lines is $\dot{e}_\alpha = \dot{e}_\beta = 0$ and the equivalent strain rate is $\dot{\varepsilon}_{\mathrm{eq}} = \dot{\Lambda}/\sqrt{3}$, where $\dot{\Lambda} = \left|\dot{\gamma}_{\alpha\beta}\right|$ denotes the equivalent shear strain rate (*cf*., *e.g*. Kachanov, 1986). Eq. (13) takes on the following form

$$\varepsilon_{\mathrm{eq}} = \Lambda/\sqrt{3} \ , \ \Lambda = \int_{s_{\mathrm{fl}}} \left(\frac{\mathrm{d}\upsilon_\alpha}{\upsilon_\beta} + \frac{\mathrm{d}\upsilon_\beta}{\upsilon_\alpha}\right), \quad (22)$$

where Λ is the equivalent shear strain and s_{fl} is the flow line.

Following Kachanov (2004) the equivalent shear strain corresponds to a shear mechanism of the plastic deformation and is applicable when studying the processes with plastic flow of metals by using the slip lines (Hill, 1950) and the evolution of damage along the slip bands (Yokobori, 1968). The equivalent strains $\varepsilon_{\mathrm{eq}}$ and Λ are correlated by a simple equation ($\varepsilon_{\mathrm{eq}} = \Lambda/\sqrt{3}$) and are equivalent.

The material accumulates the ductile strain under deep drawing as provided by the hodograph of flow lines. Initially, when the material crosses the boundary line BDC of the velocity discontinuity, the strain increases abruptly

$$\Delta\Lambda_{BDC} = \frac{\Delta\upsilon_{\beta\,BDC}}{\upsilon_{\alpha\,BDC}} = \frac{\sin\varphi_{\mathrm{d}}}{\cos(\varphi_{\mathrm{d}} - \delta_D)\cos\delta}, \quad (23)$$

where, in accordance with the hodograph, for any particle crossing the boundary BDC in the point M we may write

$$\Delta\upsilon_{\beta\,BDC} = \upsilon_0\left(\sin\varphi_{\mathrm{d}}/\cos(\varphi_{\mathrm{d}} - \delta_D)\right) \ , \ \upsilon_{\alpha\,BDC} = \upsilon_{\alpha\,M} = \upsilon_0\cos\delta \ .$$

Then a displacement of the particle within the plastic zone ABC is plotted by a segment mc of the hodograph of flow lines (Fig. 5). It allows us to determine an increase of the accumulated strain in the plastic zone ABC (up to intersection with the boundary AC)

$$\Delta\Lambda_{ABC} = \int_{s_{\mathrm{fl}}} \frac{\mathrm{d}\upsilon_{\alpha\,ABC}}{\upsilon_{\beta\,ABC}} = \int_{\delta_M}^{\delta_C} \frac{\sin\varphi_{\mathrm{d}}}{\sin\varphi_{\mathrm{d}} - \cos(\varphi_{\mathrm{d}} - \delta_D)\sin\delta}\mathrm{d}\delta \ , \quad (24)$$

where

$$\mathrm{d}\upsilon_{\alpha\,ABC} = \Delta\upsilon_{\beta\,BDC}\,\mathrm{d}\delta = \upsilon_0\left(\sin\varphi_{\mathrm{d}}/\cos(\varphi_{\mathrm{d}} - \delta_D)\right)\mathrm{d}\delta \quad \text{and}$$
$$\upsilon_{\beta\,ABC} = \Delta\upsilon_{\beta\,BDC} + \upsilon_0\sin(-\delta) = \upsilon_0\left(\left(\sin\varphi_{\mathrm{d}} - \cos(\varphi_{\mathrm{d}} - \delta_D)\sin\delta\right)/\cos(\varphi_{\mathrm{d}} - \delta_D)\right).$$

Finally, when the material particles cross the boundary line AC of the velocity discontinuity and leave the plastic zone, the strain increases abruptly again

$$\Delta\Lambda_{AC} = \frac{\Delta\upsilon_{\alpha\,AC}}{\upsilon_{\beta\,AC}} = \frac{\sin\varphi_{\mathrm{d}}\,\mathrm{ctg}(-\delta_C)}{\sin\varphi_{\mathrm{d}} - \cos(\varphi_{\mathrm{d}} - \delta_D)\sin\delta_C}, \quad (25)$$

where $\Delta\upsilon_{\alpha\,AC} = \upsilon_0\left(\sin\varphi_d/\cos\left(\varphi_d - \delta_D\right)tg\left(-\delta_C\right)\right)$, $\upsilon_{\beta\,AC} = \upsilon_0\left(\left(\sin\varphi_{\rm d} - \cos\left(\varphi_{\rm d} - \delta_D\right)\sin\delta_C\right)/\cos\left(\varphi_{\rm d} - \delta_D\right)\right)$.

The overall equivalent strain accumulated by the material particles is given by

$$\varepsilon_{\rm eq} = \Lambda/\sqrt{3} = \left(\Delta\Lambda_{BDC} + \Delta\Lambda_{ABC} + \Delta\Lambda_{AC}\right)/\sqrt{3}\,. \tag{26}$$

An increase of the strains along 3 movement trajectories $s_{\rm fl1}, s_{\rm fl2}, s_{\rm fl3}$ (*cf*., Fig. 2) of the particles with 3 different original coordinates y_0/s_0 is shown in Fig. 6. As the origin of these trajectories ($s_{\rm fl}/s = 0$) we assume their point on the boundary line *BDC* (*cf*., Fig. 2). There is always a "jump" of the strain at the plastic zone boundaries (*i.e*., at the velocity discontinuity lines).

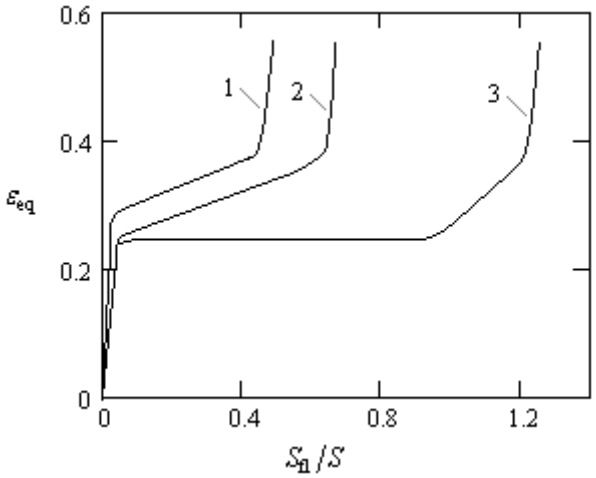

Figure 6. An increase of the strains during the material displacement within the plastic zone (for particles with the original coordinate: 1 - $y_0/s_0 = 0.2$; 2 - $y_0/s_0 = 0.32$; 3 - $y_0/s_0 = 0.67$)

Strain-induced damage of the finished part should be predicted by means of a numerical integration of the constitutive equations for the normalized measures of damage (*cf*., Zapara *et al*., 2011 for details)

$$\omega_1 = \int_0^{\varepsilon_{\rm eq}} \frac{\left[\bar{\varepsilon}_{kk}\left(\varepsilon_{\rm eq}\right)\right]'}{\bar{\varepsilon}_{\rm f}\left(\varepsilon_{\rm eq_f}\right)}{\rm d}\varepsilon_{\rm eq}\,,\ \omega_2 = \int_0^{\varepsilon_{\rm eq}} \frac{3}{\sqrt{2}}\frac{\left[\bar{\varepsilon}_{\rm eq}\left(\varepsilon_{\rm eq}\right)\right]'}{\bar{\varepsilon}_{\rm f}\left(\varepsilon_{\rm eq_f}\right)}{\rm d}\varepsilon_{\rm eq}\,, \tag{27}$$

where $\bar{\varepsilon}_{kk}$ and $\bar{\varepsilon}_{\rm eq}$ denote plastic dilatation and the equivalent deviatoric strain at meso-level (for meso-shells with voids); $\bar{\varepsilon}_{\rm f} = \left(\left(\bar{\varepsilon}_{kk\,\rm f}\right)^2 + \left(9/2\right)\left(\bar{\varepsilon}_{\rm eq_f}\right)^2\right)^{1/2}$ is the magnitude of the failure vector $\overrightarrow{O\zeta}_{\rm f}$ (see Fig. 3 in Zapara *et al*., 2011); $\bar{\varepsilon}_{kk\,\rm f}$ and $\left(3/\sqrt{2}\right)\bar{\varepsilon}_{\rm eq_f}$ are the coordinates of the vector $\overrightarrow{O\zeta}_{\rm f}$; $\varepsilon_{\rm eq_f}$ is the equivalent failure strain at macro-level; the dash refers to differentiation *w.r.t.* the parameter that governs the process of deformation (in this case *w.r.t.* $\varepsilon_{\rm eq}$).

The determination of the material functions for as-delivered pure copper was the main experimental problem in the previous paper of the authors (Zapara *et al*., 2011). The limit equivalent strain $\varepsilon_{\rm eq_f}$ depends on Stress Triaxiality (ST) and can be determined by using the experimental diagram of plasticity $\varepsilon_{\rm eq_f}\left({\rm ST}\right)$ (or, *fracture locus*) plotted for an as-delivered material studied under specified temperature-rate conditions and after recrystallization annealing (Fig. 7). The fracture locus for pure copper is based on the empirical data obtained for uniaxial tension under superimposed hydrostatic pressure by Bridgman (1964) and Pugh (1970). The empirical curves $\varepsilon_{\rm eq_f}\left({\rm ST}\right)$ can be satisfactorily described by an exponential function, $\varepsilon_{\rm eq_f} = B\exp\left[-c\left({\rm ST}\right)\right]$, where B and c are parameters defined by characteristic points on the curve $\varepsilon_{\rm eq_f}\left({\rm ST}\right)$.

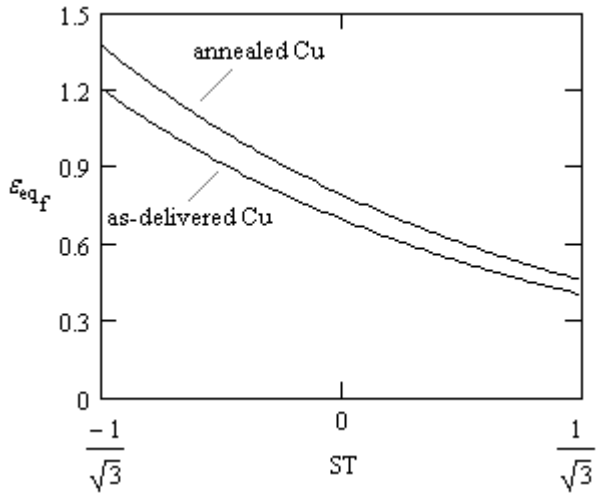

Figure 7. The fracture locus for pure copper as-delivered and after recrystallization annealing

As stated above, the material accumulates ductile damage at deep drawing as follows: initially, when it crosses the velocity discontinuity line BDC and the equivalent strain increases abruptly ($\Delta\varepsilon_{\mathrm{eq}\,BDC} = \Delta\Lambda_{BDC}/\sqrt{3}$); then, within the plastic zone ABC ($\Delta\varepsilon_{\mathrm{eq}\,ABC}$) and, finally, when it crosses the velocity discontinuity line AC and leaves the plastic zone ($\Delta\varepsilon_{\mathrm{eq}\,AC}$). Thus, the accumulated equivalent damage can be presented as below

$$\omega = \left(\omega_1^{\,2} + \omega_2^{\,2}\right)^{1/2} = \left(\left(\omega_{10} + \Delta\omega_{1\,BDC} + \Delta\omega_{1\,ABC} + \Delta\omega_{1\,AC}\right)^2 + \left(\omega_{20} + \omega_{2\,BDC} + \omega_{2\,ABC} + \omega_{2\,AC}\right)\right)^{1/2}, \qquad (28)$$

where ω_{10} , ω_{20} are the initial values of damage measures for the as-delivered material.

Figures 8 and 9 show how the damage depends on the equivalent strain for different movement trajectories of material particles with the following original coordinates: $y_0/s_0 = 0.2$; 0.32; 0.67. Pure sheet copper reveals larger ductility after recrystallization annealing as compared to its as-delivered state. Consequently, the finished shell made of annealed copper has the smaller equivalent damage ($\omega = 0.59...0.73$) than the shell made of as-delivered copper ($\omega = 0.67...0.82$). It is important to notice that the damage accumulates irregularly and with various intensity along different trajectories of material particles. This fact leads to a nonuniform distribution of the damage through the wall thickness of finished parts.

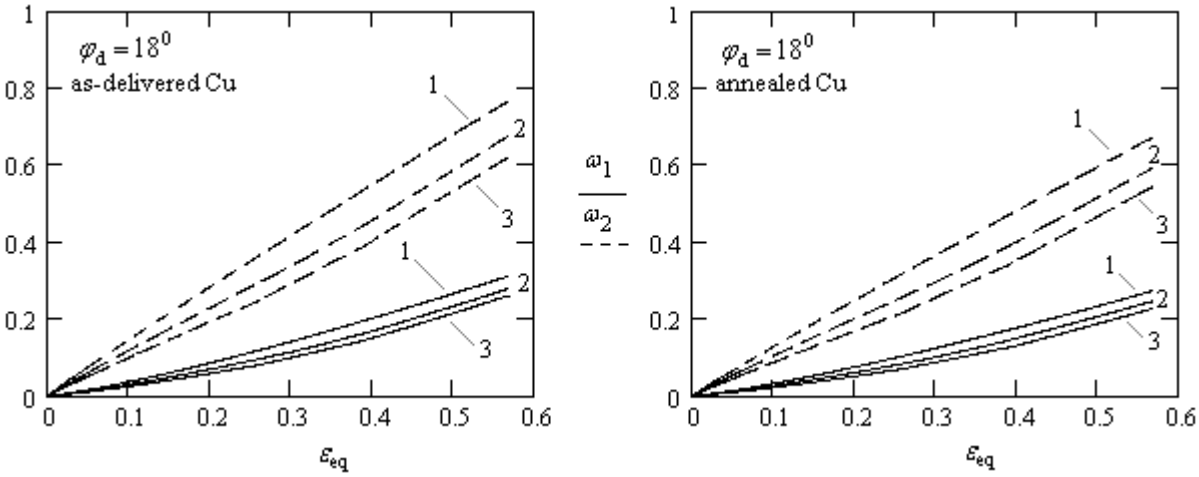

Figure 8. The damage measures ω_1 and ω_2 *vs*. the equivalent strain $\varepsilon_{\mathrm{eq}}$
(for particles with the original coordinate: 1 - $y_0/s_0 = 0.2$; 2 - $y_0/s_0 = 0.32$; 3 - $y_0/s_0 = 0.67$)

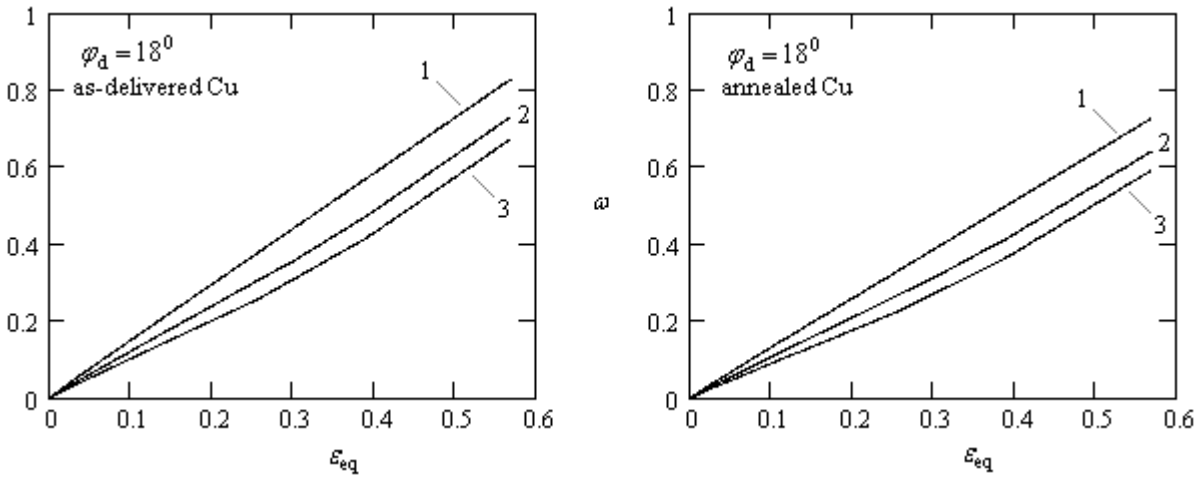

Figure 9. The equivalent damage ω *vs*. the equivalent strain ε_{eq}
(for particles with the original coordinate: 1 - $y_0/s_0 = 0.2$; 2 - $y_0/s_0 = 0.32$; 3 - $y_0/s_0 = 0.67$)

At this point we should discuss the possibility of an onset of void coalescence within the plastic zone. Fig. 10 shows how the equivalent damage at the onset of void coalescence (ω_c) depends on stress triaxiality for the case of tension of sheet pure copper with various initial void volume fraction (f_0). The curves $\omega_c(\mathrm{ST})$ were obtained from the experimental data on the ductile damage of copper specimens (*cf*., Zapara *et al*. (2011) and Pardoen *et al*., 1998). The notched specimens are used in order to attain high positive stress triaxialities $\mathrm{ST} \in \left[1/\sqrt{3};\ 2/\sqrt{3}\right]$ (*cf*., Pardoen *et al*., 1998), while negative stress triaxialities $\mathrm{ST} \in \left[-1/\sqrt{3};\ 0\right]$ can be reached by tension with superimposed hydrostatic pressure, σ_H (*cf., e.g.,* Bridgman, 1964).

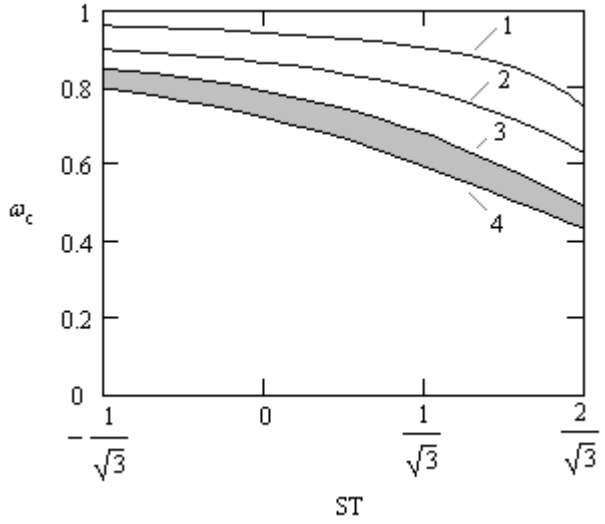

Figure 10. The equivalent damage at the onset of void coalescence (ω_c) *vs*. stress triaxiality (ST) in case of tension of sheet pure copper with various initial void volume fractions (f_0): 1, 2 – specimens without artificial defects with $f_0 = 0.002$ and 0.03, respectively; a band between the curves 3 and 4 - specimens with artificial defects (pre-drilled holes) and with $f_0 = 0.4...0.45$

From the limited experimental evidence available for pure copper it may be speculated that coalescence evolves from microscopic plastic shear localization to an intervoid necking mode followed by plastic tensile localization. The coalescence mode by microscopic shear banding can be observed by *in situ* SEM tensile testing (Pardoen *et al*., 1998). This fact proves the known analytical criterion for the onset of void coalescence based on an explicit micro-mechanical point of view and developed by Brown and Embury (1974). The dependencies $\omega_c(\mathrm{ST})$ can be quite satisfactorily approximated by the following function

$$\omega_c = \frac{1}{\pi}\operatorname{arccot}\left(K(\mathrm{ST}) - C\right), \tag{29}$$

where parameters K and C are the functions of void volume fraction (f_0) for as-delivered material

$$K = Bf_0^{(m_0 + m_1 f_0)}\ ,\ \ C = Af_0^{(n_0 + n_1 f_0)} \tag{30}$$

with $B = 0.21...0.29$, $m_0 = -0.46...-0.41$, $m_1 = -3.48...-2.12$, $A = 0.43...0.77$, $n_0 = -0.40...-0.31$, $n_1 = -1.98...0.57$. The scatter of the values of B, A, m_0, m_1, n_0, n_1 leads to a scatterband of the values of K and C.

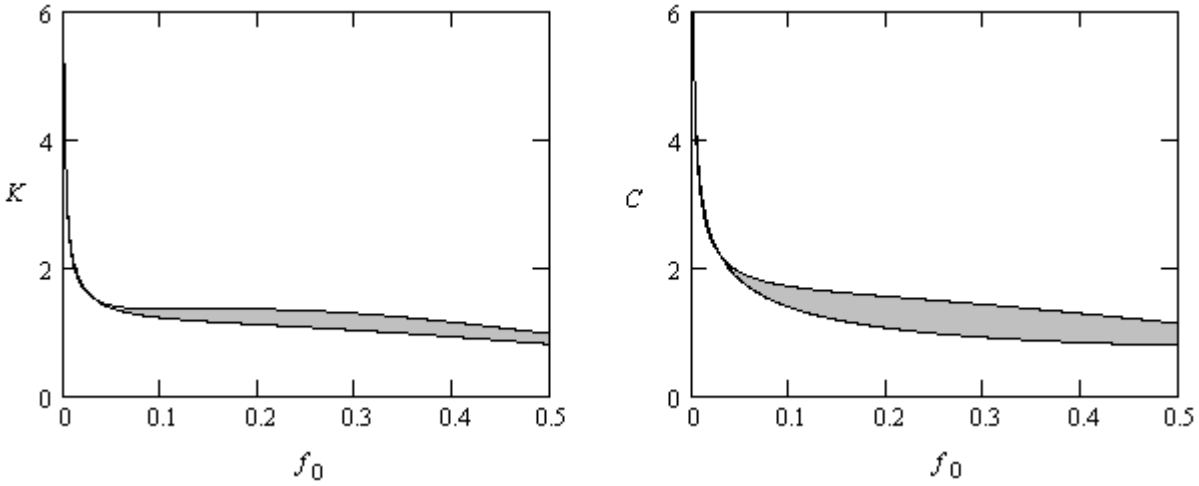

Figure 11. Parameters K and C *vs*. void volume fraction (f_0) for sheet pure copper as-delivered

The function (29) has properties that are substantial in terms of detection of the onset of coalescence: It has two asymptotes $\omega_c = 1$, $\omega_c = 0$ and the inflexion point $\mathrm{ST} = C/K$ with the extremum for the derivative $\mathrm{d}\omega_c/\mathrm{d}(\mathrm{ST})$. Asymptotic behavior of the function (29) within the range of negative stress triaxialities corresponds, from a physical point of view, to healing of microscopic defects under hydrostatic pressure ($\sigma_H < 0$). The process of void healing prevents their coalescence. Another limit of the function (29) observed within the range of positive stress triaxialities corresponds to the counter physical process related to an intensive growth of voids under tensile stresses. At high values of the initial void volume fraction this process can lead to void coalescence at the beginning of plastic deformation. Finding the location of the inflexion point for the function (29) requires further experiments aimed to extremum seeking for the derivative $\mathrm{d}\omega_c/\mathrm{d}(\mathrm{ST})$.

In the case for deep drawing of sheet pure copper with the initial void volume fraction $f_0 = 0.002$ and with stress triaxialities $\mathrm{ST} = -0.686...0.012$ the onset of coalescence occurs when the equivalent damage becomes $\omega_c = 0.94...0.96$. Predicted values of the equivalent damage in the finished part are as follows: $0.68...0.83$ for pure copper in as-delivered condition and $0.59...0.73$ for pure annealed copper (*cf*., Fig. 10). One can see that they are less than $\omega_c = 0.94...0.96$. Therefore, void coalescence does not occur in the studied process and, consequently, the finished shell will have a microscopic structure of high quality without large cavernous defects that could arise from void coalescence.

Next, we consider a possibility of reducing the strain-induced damage of the finished shell by using a drawing die with the smaller cone angle ($\varphi_d = 12^\circ...13^\circ$). In this case the plastic zone has a considerably larger extent in the area of deformation. It leads to a shift of the stress state into a range of negative stress triaxialities and, accordingly, to the larger limit strain (ε_{eq_f}) as compared to deep drawing through a die with the larger cone angle. The field of plastic flow velocities is more uniform that enables more proportional increasing of the accumulated strains.

Fig. 12 shows how the equivalent damage depends on the equivalent strain. The use of a drawing die with the smaller cone angle reduces the equivalent damage of the finished shell made of as-delivered copper from

$\omega = 0.67...0.82$ down to $\omega = 0.52...0.62$. This leads in the case of annealed copper to minimal values of the equivalent damage: $\omega = 0.45...0.55$. It is obvious that void coalescence does not occur here as well as in previous case of the larger cone angle and the finished shell will also have the microscopic structure of rather high quality.

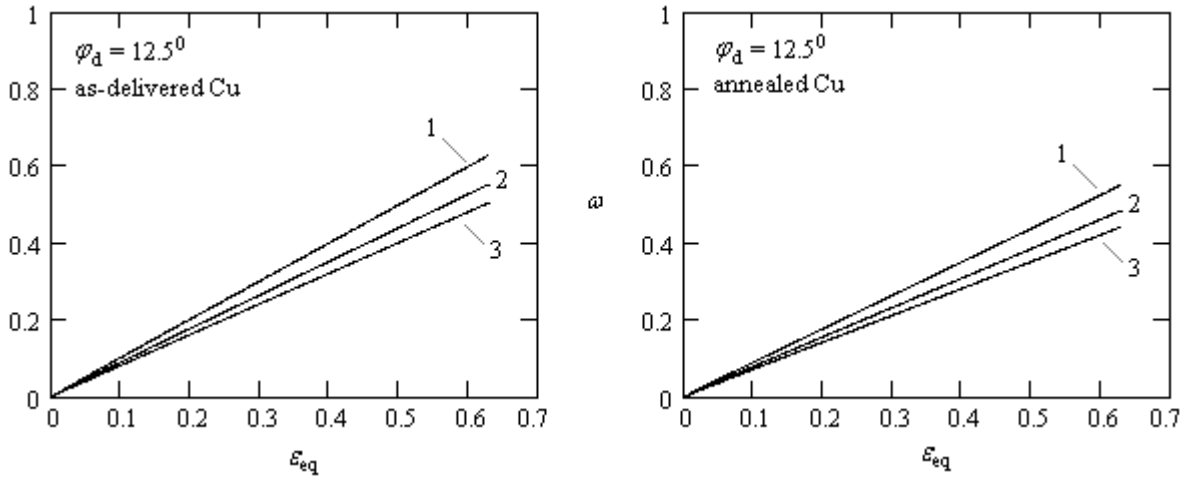

Figure 12. The equivalent damage ω *vs*. the equivalent strain ε_{eq}
(for particles with the original coordinate: 1 - $y_0/s_0 = 0.2$; 2 - $y_0/s_0 = 0.32$; 3 - $y_0/s_0 = 0.67$)

5 Prediction of Ductile Failure

Prediction of ductile failure in metal forming processes is required for the forming limit analysis. The following example shows the possibility to draw a shell with a thinner wall (s = 0.41 mm instead of s = 0.62 mm). Due to the larger final deformation a cone angle of the die is increased up to $2\varphi_d = 40^\circ$. The stress-strain state including the slip line field is determined within the plastic zone (Fig. 13) using the methods presented in Sections 2, 3, and 4. The corresponding rise of the equivalent strain along the movement trajectories $s_{fl1}, s_{fl2}, s_{fl3}$ (*cf*., Fig. 13) of the material particles with the initial coordinates $y_0/s_0 = 0.2;\ 0.32;\ 0.67$ is shown in Fig. 14 (left). The equivalent damage dependent on the equivalent strain is presented in Fig. 14 (right).

For these trajectories damage rises up to the limit value ($\omega = 1$) when the equivalent strains are equal to $\varepsilon_{eq} = 0.68;\ 0.75;\ 0.79$, which are the failure strains ε_{eq_f} for these trajectories. The points ε_{eq_f} are shown in the curves $\varepsilon_{eq}(s_{fl}/s)$ in Fig. 14 (left). They are located on straight segments of the plots which correspond to a "jump" of the strain increments. The material particles are subjected to this "jump" ($\Delta\varepsilon_{eq_{AF}}$) when crossing the velocity discontinuity line AF coinciding with the slip line α_3. Thus, the material reaches the maximum damage at the line AF which is expected to be the macro-failure trajectory outgoing from the vertex (A) of the die angle. A natural scatter of the process parameters leads to the fact that the predicted zone of failure is represented by the material layer in a neighborhood of the line AF. For example, the stochastic nature of contact friction results in a scatter of the parametric angle δ_F at the point F on the contact with a punch and, according to the parametric representation (3) of the von Mises yield condition (2), in a scatterband of the velocity discontinuity line AF (Fig. 13, shaded area). The coincidence of the predicted zone of failure with the slip bands (*i.e*., Lüders bands) corresponds to the morphology of ductile failure which is mainly governed by void nucleation, growth, and subsequent coalescence in a strongly deformed region (*cf., e.g*., Yokobori, 1968).

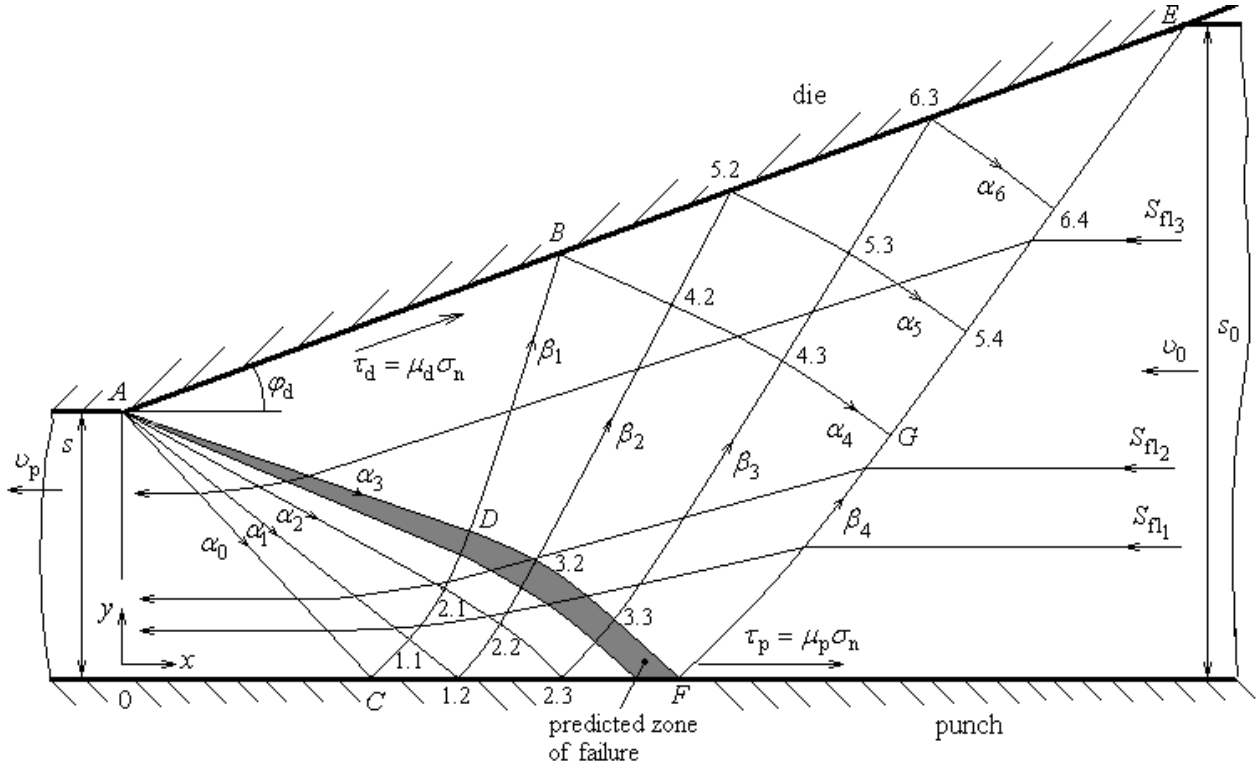

Figure 13. Plastic zone (boundary conditions, slip lines and movement trajectories of material particles) for the following initial data: $s_0/s = 2.4$, $\varphi_d = 20^\circ$, $\mu_p = 0.1$, $\mu_d = 0.09$

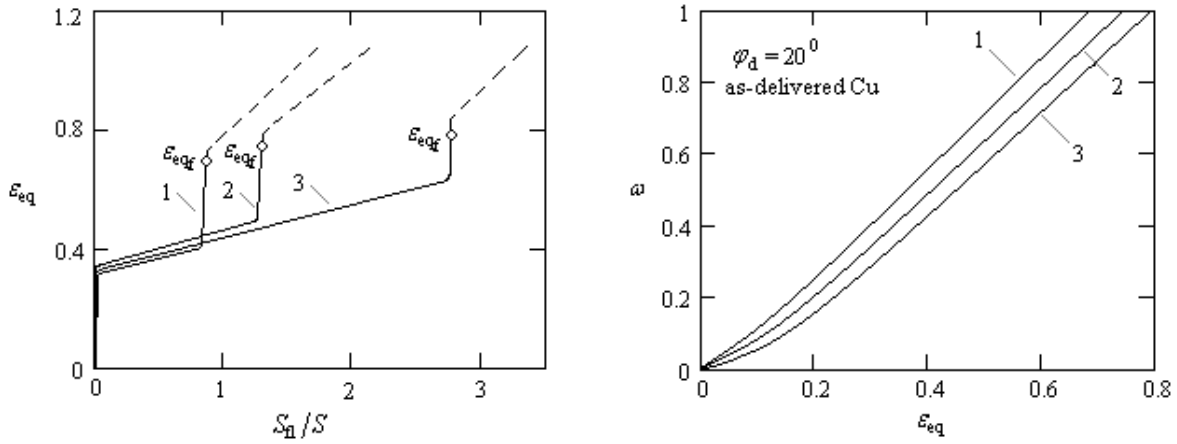

Figure 14. An increase of the equivalent strains (*left*) and the equivalent damage (*right*) during the material displacement within the plastic zone
(for particles with the original coordinate: 1 - $y_0/s_0 = 0.2$; 2 - $y_0/s_0 = 0.32$; 3 - $y_0/s_0 = 0.67$)

6 Discussion

The main problem of this study is to predict the strain-induced damage in the finished part after deep drawing. The constitutive equations of a tensorial theory for ductile damage are used for the modeling. Stresses and flow velocities which appear in these equations are determined from the solution of a mixed boundary problem (*i.e.*, when the shear stress is implicitly specified on the contact boundaries with an operating tool). The material functions were experimentally determined and presented by Zapara *et al*. (2011).

The modeling results. The diagrams for the damage measures dependent on the equivalent strain accumulated during a displacement of material particles along the trajectories within the plastic zone are plotted. An

appreciable effect of the die cone angle on the amount of damage in a finished cylindrical shell is ascertained. Reduction of this angle from $\varphi_{\mathrm{d}} = 15^{\circ}...18^{\circ}$ down to $\varphi_{\mathrm{d}} = 11^{\circ}...13^{\circ}$ leads to a shift of stress triaxialities into a range of negative values and, according to the fracture locus, to larger limit strain and lower damage. However, strong reduction of the die cone angle ($\varphi_{\mathrm{d}} = 7^{\circ}...8^{\circ}$) may lead to higher pressure from a ductile material on the contact surface of a punch and a die and, according to the friction law (13), to higher tangential friction forces. The use of annealed pure copper (instead of as-delivered) noticeably reduces damage of the finished shell as well.

We should note that the Eqs. (27) allow us to predict damage in view of changing stress triaxialities for an arbitrarily complex strain path (Fig. 6). In this case the parameters of stresses and strains which appear in Eqs. (27) should be determined with high accuracy for a studied MF process. The analysis revealed that void coalescence does not occur in the studied process of deep drawing. Void coalescence can lead to large cavernous defects and clusters and, consequently, to a "drop" in operating performance of metallic components subjected to high temperatures, pressures, and strain rates. Such products and components are widely used in aerospace, automotive and energy engineering. The development of such metal forming procedures that can provide the absence of void coalescence (*i.e.*, with $\omega < \omega_c$) is very important and, in some cases, necessary for metalware industry.

The problem of reliable prediction of ductile failure arises when studying the forming limit of the processed materials. Eqs. (27) and (28) allow us to determine for the known stress-strain state and failure locus $\varepsilon_{\mathrm{eq_f}}(\mathrm{ST})$ a set of points in the plastic region (failure zone) where the equivalent damage reaches its peak value ($\omega = 1$). In case of deep drawing of the shell with a very thin wall ($s = 0.41\,\mathrm{mm}$) the material reaches the limit damage at the velocity discontinuity line which starts from the vertex of the die angle and which is expected to be a trajectory of macroscopic failure. The substantial factor is a natural scatter of the process parameters (the stochastic nature of contact friction, a scatter of physical and mechanical properties of the material, etc.). This leads to a transformation of the predicted failure trajectory into the zone of failure (*i.e.*, a set of possible positions of this trajectory).

Drawing dies with a concave-convex generatrix of their operating contours can be used in order to reduce the extent of damage in finished parts appreciably. Devenpeck and Richmond (1965) performed a number of comparative tests for specimens which were cut from the bars drawn through different dies with conical, convex, concave, and sigmoidal profiles. Richmond and Devenpeck term such dies with a concave-convex generatrix as "sigmoidal" dies since a plane curve with one inflexion point and two parallel asymptotes is known as "sigmoid". The specimens drawn through a sigmoidal die revealed the longest fatigue life. The analysis of damage accumulated during the process of deep drawing through a sigmoidal die is one of the advanced problems in this research area.

Acknowledgement

The present work was supported by Deutsche Forschungsgemeinschaft (DFG) through the research project MU 1752/25-1.

References

Alberti, N., Barcellona, A., Cannizzaro, L., Micari, F.: Introduction of ductile fracture in metal forming processes: An approach based on the damage mechanics. *Annals of the CIRP*, 43, (1994), 207-210

Alberti, N., Barcellona, A., Masnata, A., Micari, F.: Central bursting defects in drawing and extrusion: numerical and ultrasonic evaluation. *Annals of the CIRP*, 42, (1993) 269-273

Aravas, N.: The analysis of void growth that leads to central bursts during extrusion, *J. Mech. Phys. Solids*, 34, (1986), 55-79

Bennani, B., Oudin, J.: Backward can extrusion of steels: effects of punch design on flow mode and void volume fraction. *Int. J. Mach. Tools and Manuf*., 33, (1995), 903-911

Bonora, N., Gentile, D., Pirondi, A., Newaz, G.: Ductile damage evolution under triaxial state of stress: theory and experiments. *Int. J. Plasticity*, 21, (2005), 981-1007

Boudifa, M., Saanouni, K., J.-L. Chaboche: A micromechanical model for inelastic ductile damage prediction in polycrystalline metals for metal forming. *Int. J. Mech. Sci*., 51, (2009), 453-464

Bridgman, P.W.: Studies in Large Plastic Flow and Fracture. Harvard University Press, Cambridge, MA, (1964)

Brown, L. M., Embury, J.E.: The initiation and growth of voids at second phase particles. In: *Proc. 3rd Int. Conf. Strength of Metals and Alloys*. Institute of Metals , London, (1974), 164–169

Chow, C.L., Tai, W.H., Chu, E.: Computer simulation of sheet metal forming based on damage mechanics approach. *J. Mater. Proc. Tech*., 139, (2003), 553–558

Cocks, A.C.F., Ashby, M.F.: Intergranular fracture during power-law creep under multiaxial stresses. *Met. Sci*., (1980), 395-402

Devenpeck, M., Richmond, O.: Strip-drawing experiments with a sigmoidal die profile. *J. Engng. Ind., Trans. ASME*, 87, (1965), 425–428

Geiringer, H.: Beitrag zum vollständigen ebenen Plastizitätsproblem. In: *Proc. 3rd. Int. Cong. Appl. Mech*. (Stockholm), 2, (1930), 185

Gelin, J.C., Oudin, J., Ravalard, Y.: An improved finite element method for the analysis of damage and ductile fracture in cold forming processes, *Annals of the CIRP*, 34, (1985), 209-212

Guo, Y.Q., Li, Y.M., Bogard, F., Debrey, K.,. An efficient pseudo-inverse approach for damage modeling in the sheet forming process. *J. Mater. Proc. Tech*., 151, (2004), 88–97

Gurson, A.L.: Continuum theory of ductile rupture by void nucleation and Growth Part 1 — Yield criteria and flow rules for porous ductile media. *ASME J. Engng. Mater. Techn*., 99, (1977), 2-15

Hencky, H.: Über einige statisch bestimmte Fälle des Gleichgewichts in plastischen Körpern. *Zeit. Angew. Math. Mech.*, 3, (1923), 241-251

Hill, R.: *The Mathematical Theory of Plasticity*. Oxford Univ. Press (1950)

Hsu, T.-C., Chu, C.-H., A finite element analysis of sheet metal forming processes, *J. Mater. Proc. Tech*., 54 (1995), 70-75

Hu, J.G., Ishikawa, T., Jonas, J.J.: Finite element analysis of damage evolution and the prediction of the limiting draw ratio in textured aluminum sheets. *J. Mater. Proc. Tech.*, 103, (2000), 374-382

Kachanov, L.M.: *Fundamentals of the Theory of Plasticity*. Dover Publications (2004)

Khelifa, M., Oudjene, M.: Numerical damage prediction in deep drawing of sheet metals. *J. Mater. Proc. Tech*., 200, (2008), 71-76

Kobayashi, S., Oh, S.I., Altan, T.: *Metal Forming and the Finite Element Method*. Oxford University Press, London, (1989)

Mathur, K.K., Dawson, P.R.: On modeling damage evolution during the drawing of metals. *Mech. Mater*., 6, (1987), 179-196

Needleman, A., Tvergaard, V.: An analysis of ductile rupture in notched bars. *J. Mech. Phys. Solids*, 32, (1984), 461-490

Oh, S.I., Chen, C.C., Kobayashi, S.: Ductile fracture in axisymmetric extrusion and drawing. Part 2: Workability in extrusion and drawing, *ASME J. Engng. Ind.*, 101, (1979), 36-44

Oyane, M., Sato, T., Okimoto, K., Shima, S.: Criteria for ductile fracture and their applications, J . *Mech. Work. Tech*., 4, (1980), 65-81

Pardoen, T., Doghri, I., Delannay, F.: Experimental and numerical comparison of void growth models and void coalescence criteria for the prediction of ductile fracture in copper bars. *Acta Mater*., 46, (1998), 541-552

Prager, W., Hodge, P. G.: *Theory of Perfectly Plastic Solids*. New York, Wiley (1951)

Pugh, H.L.D.: *Mechanical Behaviour of Materials under Pressure*. Elsevier, London (1970)

Reddy, N.V., Dixit, P.M., Lal, G.K.: Ductile fracture criteria and its prediction in axisymmetric drawing. *Int. J. Mach. Tools & Manuf.*, 40, (2000), 95–111

Tang, J., Wu, W.T., Walters, J.: Recent developments and applications of finite element method in metal forming, *J. Mater. Proc. Tech.*, 46, (1994), 117–126

Wang, N.M., Budiansky, B.: Analysis of sheet metal stamping by a finite element method. *ASME J. Appl. Mech*., 100, (1978), 73-82

Woo, D.M.: The stretching forming test. *The Engineer*, 200, (1965), 876-880

Yokobori, T.: *An Interdisciplinary Approach to Fracture and Strength of Solids*. Gordon & Breach, Pub. New York (1968)

Zapara, M.A., Tutyshkin, N.D., Müller, W.H., Wille, R.: A Study of Ductile Damage and Failure of Pure Copper – Part I: Constitutive Equations and Experiments. *Tech. Mech.*, 31 (2), (2011), 132-155.

Addresses: Dr. M. Zapara, Prof. Dr. W. H. Müller, Dr. R. Wille, Lehrstuhl für Kontinuumsmechanik und Materialtheorie, Technische Universität Berlin, Sekretariat MS 02, Einsteinufer 5, D-10587 Berlin, Germany.
E-mail: Maksim.Zapara@tu-berlin.de, Wolfgang.H.Mueller@tu-berlin.de, Ralf.Wille@tu-berlin.de,
Prof. Dr. N. Tutyshkin, Lehrstuhl für Bauwesen, Baustoffe und Baukonstruktionen, Universität Tula, 300600 Tula, Russland. E-mail: tutyshkin@mail.ru